Degradation of GaN-Based Multiple Quantum Wells Solar Cells Under Forward Bias: Investigation Based on Optical Measurements and Steady-State Photocapacitance

Alessandro Caria, Carlo De Santi, *Member, IEEE*, Matteo Buffolo, *Member, IEEE*, Marco Nicoletto, *Student Member, IEEE*, Xuanqi Huang, Houqiang Fu, *Member, IEEE*, Hong Chen, Yuji Zhao, Gaudenzio Meneghesso, *Fellow, IEEE*, Enrico Zanoni, *Life Fellow, IEEE*, and Matteo Meneghini, *Senior Member, IEEE*

***Abstract*—Gallium nitride (GaN) multiple quantum well (MQW) solar cells proved to have very good performance in high-temperature conditions and under intense excitation. However, the long-term reliability under harsh conditions has not been investigated in the literature. The aim of this article is to fill this gap, by investigating the degradation mechanisms of GaN solar cells, submitted to forward current stress. The cells were characterized by means of dark and illuminated current–voltage (*I*–*V*) measurements, capacitance–voltage (*C*–*V*) measurements, and steady-state photocapacitance (SSPC). The current step-stress experiment showed an initial decrease in the main parameters of the devices (open-circuit voltage, external quantum efficiency (EQE), and optical-to-electrical power conversion efficiency). *C*–*V* and SSPC showed a correlation between the charge inside the active region of the device and the concentration of trap states. Also, a relation was found between the decrease in power conversion efficiency and the amount of charge in the active region of the devices. Degradation was ascribed to a redistribution of the charge in the active region, related to an increase in the density of midgap states (E_C – 1.6 eV), resulting in the lowering of the efficiency of the devices.**

***Index Terms*—Gallium nitride (GaN), photodetectors, reliability, solar cells.**

Manuscript received 28 March 2023; accepted 24 April 2023. Date of publication 26 May 2023; date of current version 21 June 2023. This work was supported in part by European Union–Next Generation EU, within the Piano Nazionale di Ripresa e Resilienza (PNRR) Project "NEST–Network 4 Energy Sustainable Transition" for the activity at the University of Padova; and in part by Ultra Materials for a Resilient, Smart Electricity Grid (ULTRA), an Energy Frontier Research Center (EFRC) funded by the U.S. Department of Energy, Office of Science, Basic Energy Sciences for the work at Arizona State University and Rice University under Award DE-SC0021230. The review of this article was arranged by Editor C. Surya. *(Corresponding author: Alessandro Caria.)*

Alessandro Caria, Carlo De Santi, Matteo Buffolo, Marco Nicoletto, Gaudenzio Meneghesso, and Enrico Zanoni are with the Department of Information Engineering, University of Padova, 35131 Padua, Italy (e-mail: alessandro.caria@unipd.it).

Xuanqi Huang, Houqiang Fu, Hong Chen, and Yuji Zhao are with the School of Electrical, Computer, and Energy Engineering, Arizona State University, Tempe, AZ 85287 USA.

Yuji Zhao is with the School of Electrical, Computer, and Energy Engineering, Arizona State University, Tempe, AZ 85287 USA, and also with the Department of Electrical and Computer Engineering, Rice University, Houston, TX 77005 USA.

Matteo Meneghini is with the Department of Information Engineering and the Department of Physics and Astronomy, University of Padova, 35131 Padua, Italy.

Color versions of one or more figures in this article are available at https://doi.org/10.1109/TED.2023.3272297.

Digital Object Identifier 10.1109/TED.2023.3272297

I. Introduction

Gallium nitride (GaN) is now the semiconductor of choice for many optoelectronic applications in the visible and UV spectral ranges. The availability of small, efficient, and reliable InGaN LEDs allows fabricating blue and white light-emitting diodes, that are now massively penetrating the application market. Also, the photovoltaic sector can take advantage of this material [1], [2]: the use of GaN in solar cells allows to exploit the blue-UV region of the solar spectrum [3], by tuning the composition of the InGaN alloy [4]. GaN could then be used in multijunction solar cells as an additional junction to increase the efficiency, in silicon-GaN tandem solar cells [5], [6], in stand-alone solar cells, or for fabricating photodetectors for wireless power transfer systems [7], [8]. In all cases, the use of GaN can lead to a substantial improvement in the efficiency of the solar cells/detectors and is therefore subject to intense investigation.

Recently, GaN solar cells [9], in particular devices based on multiple quantum well (MQW) structures, proved to have good performance also under high optical powers and under high temperatures [10], [11], thus being potential candidates for applications in concentrator photovoltaic systems and in the space environment [12]. However, very few reports investigated the degradation processes of this kind of device. Preliminary reports investigated the degradation of cells submitted to thermal [13] or optical stress [14], [15], while the electrically driven degradation processes are relatively unexplored. There are few reports on current stress on this kind of device; these reports do not focus on the analysis of the photovoltaic properties and their relation with the newly

0018-9383 © 2023 IEEE. Personal use is permitted, but republication/redistribution requires IEEE permission.
See https://www.ieee.org/publications/rights/index.html for more information.

Authorized licensed use limited to: Fondren Library Rice University. Downloaded on August 24,2023 at 15:03:13 UTC from IEEE Xplore. Restrictions apply.

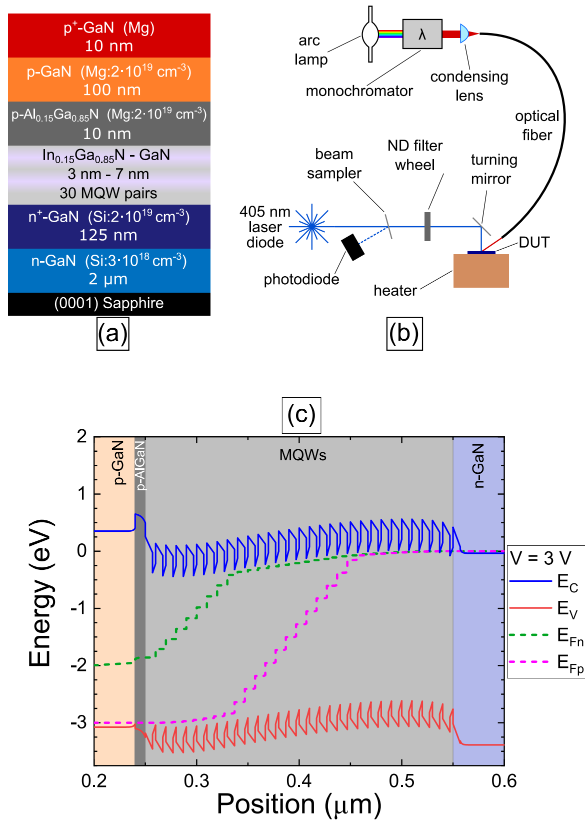

Fig. 1. (a) Device structure, (b) experimental setup, and (c) simulated band diagram at 3 V.

created defects [16], [17]. The aim of this article is to fill this gap, by contributing to the understanding of the processes responsible for the degradation of InGaN-GaN MQW solar cells submitted to high current stress, and on the analysis of the link with the photovoltaic properties of the devices.

To this aim, we carried out a set of degradation tests in forward bias, i.e., in a condition where a large current density flows through the devices, in the absence of optical excitation. This helps understand which degradation mechanisms are activated by the carrier flow. We performed a step-stress experiment, by increasing the current until the device failed, and a 100 h constant-current stress at a current density high enough to induce degradation, chosen according to step-stress results. During the forward bias step stress, a variation in charge density in the active region of the device was found, well correlated with the variation in defect density detected by steady-state capacitance measurements. During the constant current stress, the decrease in the optical-to-electrical power conversion efficiency was found to be well correlated with the change in the charge integral in the active region.

II. Devices and Methods

The devices under test (DUT) are 1×1 mm^2 solar cells and their structure is schematically shown in Fig. 1(a). On (0001) Sapphire, a 2 μm n-GaN layer (3×10^{18} cm^{-3} silicon doping) and a 125 nm n$^+$-GaN layer (2×10^{19} cm^{-3} silicon doping) are grown. The active region consists of $30 \times$ In$_{0.15}$Ga$_{0.85}$N (3 nm)–GaN (7 nm) MQW structure, topped by a 10 nm p-Al$_{0.15}$Ga$_{0.85}$N layer (2×10^{19} cm^{-3} magnesium doping), a 100 nm p-GaN layer (2×10^{19} cm^{-3} magnesium doping) and a 10 nm p$^+$-GaN layer (magnesium doped). 1×1 mm^2 solar cells are processed by standard lithography and a 120 nm indium-tin-oxide (ITO) layer is deposed as a semitransparent current spreading layer, whereas Ti/Al/Ni/Au and Ti/Pt/Au contacts are formed for cathode and anode, respectively. Further details are available in [18].

The devices were characterized by means of dark and illuminated I–V, measured by a semiconductor parameter analyzer. A 405 nm laser diode was used as a light source for illuminated characterizations. A portion of the laser beam was redirected by a beam sampler to a photodiode to have optical feedback of the laser beam power. The laser beam passed through a series of neutral optical density absorptive filters to obtain low excitation powers and was then directed onto the sample by a mirror. An *LCR* meter was used for C–V and SSPC measurements. The latter was performed by using a 300-W Xenon arc-lamp source; wavelength selection was obtained by a grating monochromator. The output of the monochromator was focused on an optical fiber to be shined onto the sample. A preliminary simulation of the structure was performed by Synopsys Sentaurus TCAD software, obtaining the band diagram at 3 V shown in Fig. 1(c). It is possible to see the periodic structures of the 30 quantum wells in the middle and the AlGaN electron blocking layer on the left, at around 0.25 μm.

III. Results and Discussion

A. Step-Stress Experiment

To evaluate the degradation limits of the samples, a step-stress experiment was performed in forward bias on a representative device. The stress current was increased from 0.5 to 3 A/cm^2 in 0.5 A/cm^2 steps, from 3 to 15 A/cm^2 in 1 A/cm^2 steps, and from 15 to 50 A/cm^2 (when the device failed) in 2.5 A/cm^2 steps; the duration of each step of the stress was set to 30 min. The device was characterized by dark and illuminated I–V, with excitation densities ranging from 9.43 μW/cm^2 to 471 W/cm^2, by C–V measurements and by steady-state photocapacitance (SSPC) analysis. SSPC measurements allow to evaluate the density of trap levels, since monochromatic light stimulates the emission of trapped carriers from the deep levels, resulting in a proportional change in the capacitance of the junction. SSPC measurements were performed at 0 V with an initial dark phase of 300 s, an illuminated phase of 100 s and a 10 s forward bias pulse (3 V) in dark conditions to repopulate deep levels, by using the method presented by Armstrong et al. [19].

As shown in Fig. 2(a), by increasing the stress current an increase in forward voltage was observed. In the last steps ($I > 30$ A/cm^2), a very high voltage drop in the initial phase of the stress (higher than 1 V in the very last steps) that can be ascribed to the strong self-heating of the device. Eventually, the device fails and stress voltage reaches the compliance level. In Fig. 2(b) and (c) dark I–V characterizations after each step of the stress and series resistance calculated from these measurements are shown. In the first steps of the stress (up to 25 A/cm^2) the device shows a gradual degradation as an increase in reverse leakage and a significant increase in low forward bias current, possibly due to enhancement in trap-assisted tunneling (TAT) mechanisms [20], [21]. At 27.5 A/cm^2 there is a creation of a

Authorized licensed use limited to: Fondren Library Rice University. Downloaded on August 24,2023 at 15:03:13 UTC from IEEE Xplore. Restrictions apply.

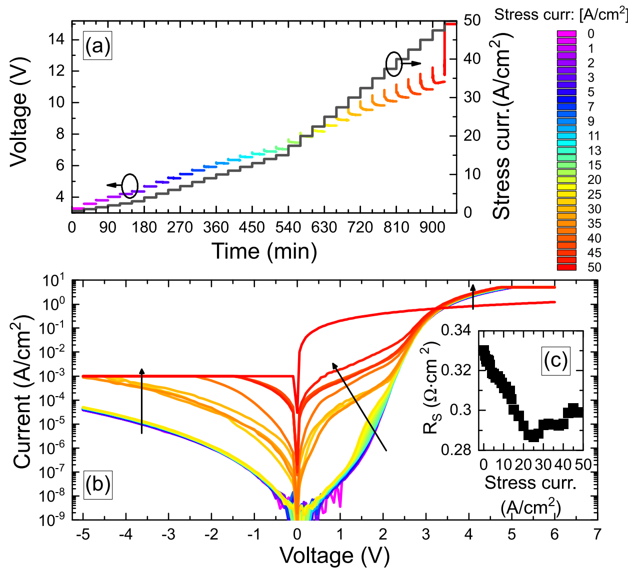

Fig. 2. (a) Stress voltage with respect to stress time and stress current. (b) Dark I–V characterizations after each step of the step-stress. (c) Series resistance estimated from dark I–V characterization.

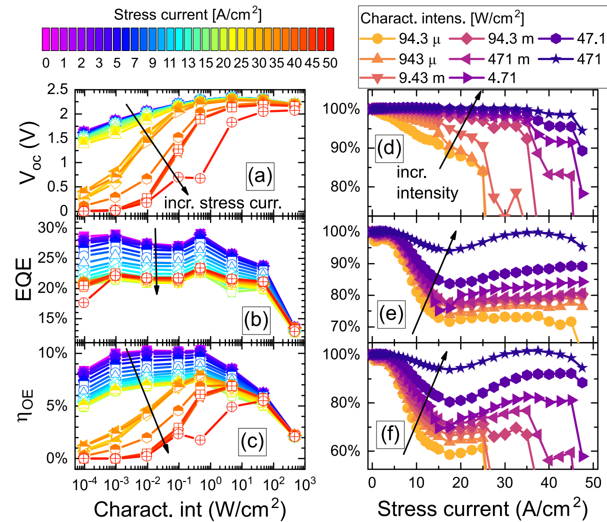

Fig. 3. Photovoltaic parameters calculated from illuminated I–V characterizations during step-stress experiment. (a) Open-circuit voltage, (c) EQE at 405 nm, and (e) optical-to-electrical power conversion efficiency at 405 nm with respect to characterization intensity at different stress currents. (b) Open-circuit voltage, (d) EQE at 405 nm, and (f) optical-to-electrical power conversion efficiency at 405 nm with respect to stress current, normalized by the unstressed value, at different characterization intensities.

huge shunt path, that increases in the following steps of stress, until the device failure at 50 A/cm^2 current density, showing a resistive behavior. During the stress, there is a decrease in series resistance up to 25 A/cm^2 stress current, followed by a slight increase. This process can be ascribed to the competition between the increase in the dopant activation in the p- or p$^+$-GaN layer, which prevails in the first part of the stress [22], and the degradation of the contact on the p-side, that is possibly stronger at higher stress currents [23], [24].

From illuminated I–V characterizations the main device parameters have been calculated, including the efficiency. The external quantum efficiency (EQE) at 405 nm is defined as the ratio between the number of carriers extracted (per unit time) $n_{\text{electrons}}$ from the device in short-circuit conditions and the number of injected photons (per unit time) n_{photons}, i.e.,

$$\text{EQE} = \frac{n_{\text{electrons}}}{n_{\text{photons}}} = \frac{h \cdot c}{P_{\text{optical}} \cdot \lambda} \cdot \frac{J_{\text{SC}} \cdot A}{q} \quad (1)$$

where h is the Planck constant, c is the speed of light, J_{SC} is the short-circuit current density, A is the area of the device, P_{optical} is the optical power delivered to the device, λ is the wavelength of the light, and q is the electron charge.

The optical-to-electrical power conversion efficiency (η_{OE}) at 405 nm is defined as the ratio between the maximum power extracted from the device $P_{\text{electrical,MAX}}$ and the excitation of optical power

$$\eta_{\text{OE}} = \frac{P_{\text{electrical,MAX}}}{P_{\text{optical}}}. \quad (2)$$

Open-circuit voltage V_{OC}, shown in Fig. 3(a), increases logarithmically with increasing excitation, until a maximum is reached, then decreases. The logarithmic increase can be explained by taking into account the standard Shockley diode equation. In open-circuit conditions ($V = V_{\text{OC}}$), the voltage is

$$V_{\text{OC}} = \frac{k_B T}{q} \ln\left(1 + \frac{I_L}{I_S}\right) \quad (3)$$

where k_B is Boltzmann's constant, T is the temperature, I_L is the photogenerated current, and I_S is the reverse saturation current. The deviation from this behavior can be attributed to the quantum structure since the carriers are confined inside the quantum wells in open-circuit condition: V_{OC} can increase with increasing levels of excitation until there are available states inside the quantum wells, then band-filling effects prevent open-circuit voltage to further increase and eventually self-heating at very high excitation densities causes V_{OC} to decrease [25], [26]. Looking at the degradation dynamics of the open-circuit voltage by increasing stress current, shown in Fig. 3(b), it is possible to see that the degradation is stronger at low characterization intensities. The gradual degradation seen up to 25 A/cm^2 can be related to an increase in defect density in the active region, which increases the recombination rate, thus lowering the open-circuit voltage and affects more the V_{OC} at low excitation densities. The shunt seen in dark I–V characterizations heavily affects open-circuit voltage, since a part of the potential drop across the device occurs through this low-resistance path.

The EQE as a function of excitation density, plotted in Fig. 3(c), has a nearly flat profile at low and intermediate excitation densities and decreases at high excitation densities. This may be ascribed to the effect of series resistance since the EQE is calculated from the short-circuit current [see (1)], that at high excitations is over 1 A/cm^2. The plot of EQE as a function of stress current [Fig. 3(d)] has an initial stable phase (up to 5 A/cm^2), then a decrease (up to 17.5 A/cm^2), and then an increase, possibly due to the variation in recombination rate in the active zone of the device. The conversion efficiency with respect to characterization intensity [Fig. 3(e)] increases with increasing excitation, as V_{OC}, has a maximum for intermediate excitation values and then decreases at high excitation intensities, as EQE. This is due to the fact that the carriers are partially confined inside the quantum wells, thus at low excitation densities recombination subtracts carriers from

Authorized licensed use limited to: Fondren Library Rice University. Downloaded on August 24,2023 at 15:03:13 UTC from IEEE Xplore. Restrictions apply.

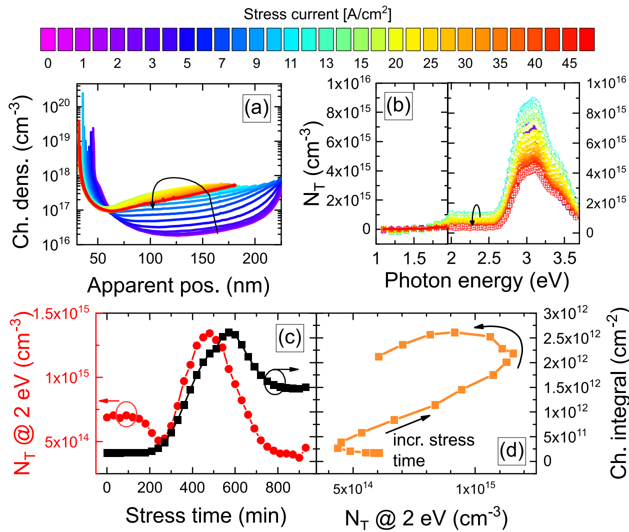

Fig. 4. (a) Charge density with respect to the position calculated from C–V measurements. (b) Trap density with respect to photon energy. (c) Charge integral in the region 75 ÷ 150 nm (black) and trap level density at 2 eV (red) with respect to stress time. (d) Correlation between charge integral and trap level density at 2 eV (orange solid line).

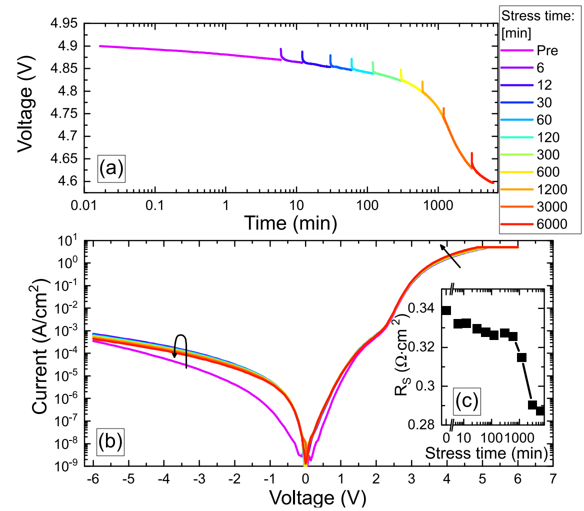

Fig. 5. (a) Stress voltage with respect to stress time, (b) dark I–V characterizations after each step of the stress, and (c) series resistance estimated from the dark I–V characterization during constant current stress at 4 A/cm^2.

being extracted from the device. On the other hand, at high excitation densities the series resistance, parasitic conduction, and band-filling effects decrease the efficiency. The η_{OE} with respect to the stress current, shown in Fig. 3(f), has a behavior very similar to the EQE. Device shunt resistance, observed at 25 A/cm^2 heavily affects η_{OE} at low excitation densities, whereas efficiency at high excitation densities does not change.

In Fig. 4(a), the calculated charge profile with respect to the apparent position calculated from C–V measurements is plotted. We detected an initial phase in which charge density profiles do not change (up to 3 A/cm^2 stress current), a second phase with a significant variation in these profiles (up to 20 A/cm^2 stress current), and a third phase in which the evolution of the charge profile is reversed. The unstressed device showed a very high charge density in the region around 50 nm, then a decrease in the charge with a large valley in the region between 75 and 200 nm. The valley is ascribed to the (low-doping) MQW region. Stress was found to induce an increase in the density of charge in the quantum well region, followed by stabilization.

By looking at the trap level concentration calculated from SSPC measurements with respect to the photon energy [Fig. 4(b)] it is possible to see two steps in the curve: a first step around 1.6 eV and a second step around 2.65 eV (the latter corresponding to the absorption on the quantum wells). As can be noticed, stress induced an increase in the density of traps within the active region of the devices, especially around 1.6 eV, which corresponds to the emission from a near-midgap deep level. These deep levels are known to be effective Shockley–Read–Hall (SRH) recombination centers, since the SRH recombination rate R_{SRH} in an intrinsic region, can be considered proportional to [27]

$$R_{\mathrm{SRH}} \propto \left[1+\cosh\left(\frac{E_T-E_{F_i}}{k_B T}\right)\right]^{-1} \tag{4}$$

where E_{F_i} is the intrinsic Fermi level energy and E_T is the trap-level energy. Possible sources of effective nonradiative recombination centers in InGaN can be nitrogen vacancies [28], [29], complexes of gallium vacancies [30] or divacancies [31], [32], [33].

From the charge density profile, the charge density integral in the region between 75 and 150 nm (the quantum well region) was calculated and plotted in Fig. 4(c) (black line) with the trap level density at 2 eV (red line). Both exhibit a peak during the stress, that is slightly shifted, due to the fact that SSPC and charge integral are measured in different regions of the device. This is evident also by the curve in Fig. 4(d), where there is an almost linear correlation between charge integral and trap level density; the nonperfect alignment of the curves is due to the slightly different region under analysis. These results suggest that a charge rearrangement is happening in the device, which also causes a variation in the density of trap levels. Since the apparent charge profile in Fig. 4(a) is referred to the (weakly n-type) quantum well region, we can infer that stress induces the propagation of defects within the active region of the devices. Such defects may create both a state near midgap ($E_C - 1.6$ eV), which is visible through SSPC measurement, and a shallow donor state, which is responsible for the variation in free carrier density reported in Fig. 4(c).

Thus, the EQE and conversion efficiency variation can be attributed to a variation in recombination in the active region due to defect migration. This also affects open-circuit voltage, lowering it during the stress: the charge increase in the active layers should lead to an increased open-circuit voltage, but the overall effect is a decrease in V_{OC} due to enhanced recombination through midgap states [34]. In the second part of the stress (for currents higher than 25 A/cm^2) no recovery is visible due to the shunt of the device, which heavily impacts on V_{OC} (and η_{OE} at the lowest excitation densities).

B. Constant Current Stress Experiment

Based on the data of the step-stress, a constant current stress was performed on another fresh device, by choosing a stress current density of 4 A/cm^2 to obtain a measurable amount of degradation in a reasonable time. The stress voltage as a function of time is plotted in Fig. 5(a). A slight decrease in the voltage was observed at the beginning of the stress, that is due to the self-heating of the device, followed by a

Authorized licensed use limited to: Fondren Library Rice University. Downloaded on August 24,2023 at 15:03:13 UTC from IEEE Xplore. Restrictions apply.

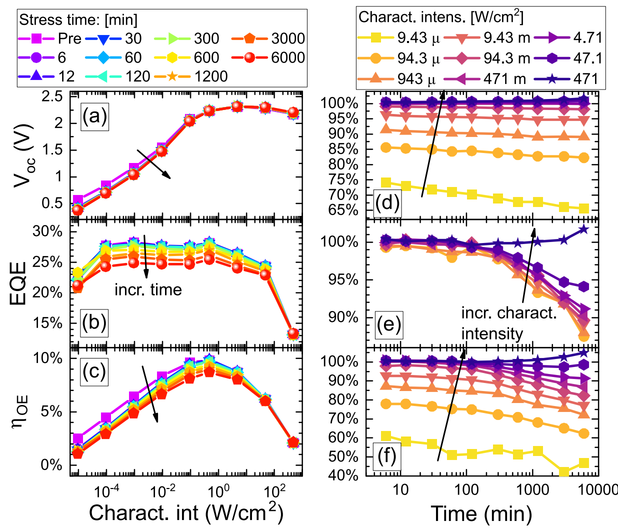

Fig. 6. Photovoltaic parameters calculated from illuminated I–V characterizations during constant stress experiment. (a) ppen-circuit voltage, (c) EQE at 405 nm, and (e) optical-to-electrical power conversion efficiency at 405 nm with respect to characterization intensity at different stress times. (b) Open-circuit voltage, (d) EQE at 405 nm, and (f) optical-to-electrical power conversion efficiency at 405 nm with respect to stress time, normalized by the unstressed value, at different characterization intensities.

stronger decrease in the voltage during the stress, in particular in the last 5000 min of the stress. This decrease in the three last steps can be ascribed to a decrease in series resistance [Fig. 5(c)]. The dark I–V characterizations [in Fig. 5(b)] show an initial increase in leakage, that is gradually recovered during the stress. In forward bias conditions, there is a two slope behavior of the I–V curve: in the region up to 2.5 V there is an inflection, seen also in the other device, due to trap-assisted conduction mechanisms, and above 2.5 V there is the conduction from the main diode, limited by series resistance [20], [21].

In Fig. 6, the operating parameters of the device calculated from illuminated I–V characterizations during the stress are reported. As expected, the constant current stress induces a gradual degradation, rather than the catastrophic degradation observed in the step-stress. However, degradation kinetics are similar: we observed a decrease in open-circuit voltage at low excitation densities, as reported in Fig. 6(a) and (c), with an initial decrease that corresponds to the variation observed in the dark I–V characterization. Also, the EQE decreases during the stress, as reported in Fig. 6(b) and (e). This decrease is not related to the series resistance variation, except for the highest characterization intensity, since the observed decrease in series resistance should result in an increase of the EQE.

The optical-to-electrical power conversion efficiency [Fig. 6(c) and (f)] decreased with increasing stress time at low excitation densities, especially in the first step of the stress, and increased in the last steps of the stress at the highest characterization intensities. This increase is related to the lowering in series resistance.

In Fig. 7(a) the calculated charge profile is plotted. Degradation kinetics were similar to those observed in the step-stress experiment: measurements revealed a gradual change in the capacitance during the stress, which is related to an increase in charge density in the MQW region. In this case, as observed in the illuminated I–V characterization results, the amount of degradation is lower than in the step-stress experiment and there is no recovery in the degradation. Trap density calculated

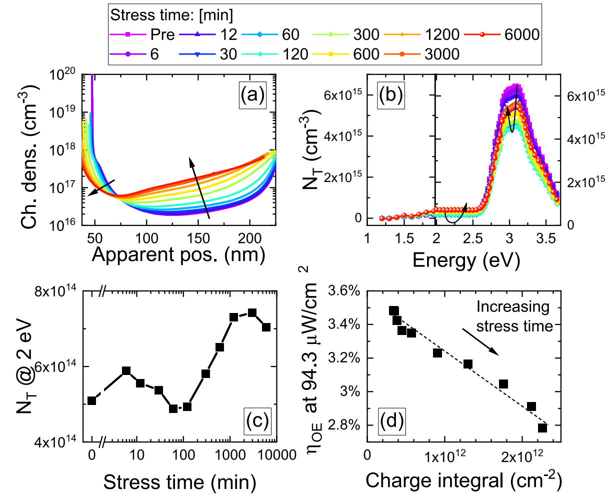

Fig. 7. (a) Charge density with respect to the position calculated from C–V measurements, (b) trap-level density with respect to photon energy, (c) trap level density at 2 eV with respect to stress current calculated from SSPC and C–V measurements and (d) correlation between power conversion efficiency at 94.3 μW/cm^2 and charge integral in the region 75 ÷ 150 nm. Dashed line is a guide for the eye.

from SSPC measurements [Fig. 7(b)] showed an increase in deep-level concentration, with an energy of around 1.6 eV. Similar to the step stress, the initial concentration of trap levels is 6×10^{14} cm^{-3}, and it increases until a maximum is reached [Fig. 7(c)]. However, during the step stress experiment the maximum was 1.4×10^{15} cm^{-3}, whereas during the stress the increase is very moderate, up to 7×10^{14} cm^{-3}. This suggests that current flow promotes the creation of new deep levels in the active region of the device with the same energy as preexisting deep levels, proportionally to its magnitude. However, this process seems to revert when the device is submitted to very high currents. The charge integral in the region between 75 and 150 nm was well correlated with the decrease in conversion efficiency [see Fig. 7(d)]. Since charge integral is, in its turn, correlated with the increase in trap density, it is possible to conclude that the creation of defects in the active zone, due to the migration of free charge, increases the nonradiative recombination ratio, thus lowering conversion efficiency during the stress.

IV. Conclusion

In conclusion, we analyzed the degradation of MQW GaN solar cells submitted to forward current step stress and constant current stress. The degradation showed a decrease in the main cell parameters (open-circuit voltage, EQE, and conversion efficiency) of the devices, especially at low excitation densities. C–V and SSPC characterizations showed that the variation in charge integral in the active region of the device and the trap level density are correlated, thus the degradation is ascribed to the redistribution of charge in the MQW region of the device and the generation of trap levels, both shallow states and deep levels, the latter with energies near 1.6 eV, i.e., near the midgap, that enhance parasitic recombination. Very high-stress currents cause the shunt of the devices, dramatically lowering the short-circuit voltage and the efficiencies, but this shunt is not observed when stressing the device at moderate current levels. In summary, the main outcome of current stress is the migration of charge in the active zone of the device, causing an increase in the concentration of deep levels that lowers power conversion efficiency.

Authorized licensed use limited to: Fondren Library Rice University. Downloaded on August 24,2023 at 15:03:13 UTC from IEEE Xplore. Restrictions apply.

ACKNOWLEDGMENT

The views and opinions expressed are, however, only those of the authors and do not necessarily reflect those of the European Union or the European Commission. Neither the European Union nor the European Commission can be held responsible for them.

REFERENCES

[1] A. G. Bhuiyan, K. Sugita, A. Hashimoto, and A. Yamamoto, "InGaN solar cells: Present state of the art and important challenges," *IEEE J. Photovolt.*, vol. 2, no. 3, pp. 276–293, Jul. 2012, doi: 10.1109/JPHOTOV.2012.2193384.

[2] D. V. P. McLaughlin and J. M. Pearce, "Progress in indium gallium nitride materials for solar photovoltaic energy conversion," *Metall. Mater. Trans. A*, vol. 44, no. 4, pp. 1947–1954, Apr. 2013, doi: 10.1007/s11661-013-1622-1.

[3] R. M. Farrell et al., "High quantum efficiency InGaN/GaN multiple quantum well solar cells with spectral response extending out to 520 nm," *Appl. Phys. Lett.*, vol. 98, no. 20, May 2011, Art. no. 201107, doi: 10.1063/1.3591976.

[4] P. G. Moses and C. G. Van de Walle, "Band bowing and band alignment in InGaN alloys," *Appl. Phys. Lett.*, vol. 96, Jan. 2010, Art. no. 021908, doi: 10.1063/1.3291055.

[5] L. A. Reichertz, I. Gherasoiu, K. M. Yu, V. M. Kao, W. Walukiewicz, and J. W. Ager, "Demonstration of a III–nitride/silicon tandem solar cell," *Appl. Phys. Exp.*, vol. 2, no. 12, Dec. 2009, Art. no. 122202, doi: 10.1143/APEX.2.122202.

[6] N. Laxmi, S. Routray, and K. P. Pradhan, "III-nitride/Si tandem solar cell for high spectral response: Key attributes of auto-tunneling mechanisms," *Silicon*, vol. 12, pp. 1–9, Dec. 2019, doi: 10.1007/s12633-019-00342-y.

[7] L. Summerer and O. Purcell, "Concepts for wireless energy transmission via laser," in *Proc. Int. Conf. Space Opt. Syst. Appl. (ICSOS)*, 2009, pp. 1–9.

[8] C. De Santi et al., "GaN-based laser wireless power transfer system," *Materials*, vol. 11, no. 1, p. 153, 2018, doi: 10.3390/ma11010153.

[9] Y. Zhao et al., "Toward high efficiency at high temperatures: Recent progress and prospects on InGaN-based solar cells," *Mater. Today Energy*, vol. 31, Jan. 2023, Art. no. 101229, doi: 10.1016/j.mtener.2022.101229.

[10] R. Dahal, J. Li, K. Aryal, J. Y. Lin, and H. X. Jiang, "InGaN/GaN multiple quantum well concentrator solar cells," *Appl. Phys. Lett.*, vol. 97, no. 7, Aug. 2010, Art. no. 073115, doi: 10.1063/1.3481424.

[11] G. Moses, X. Huang, Y. Zhao, M. Auf der Maur, E. A. Katz, and J. M. Gordon, "InGaN/GaN multi-quantum-well solar cells under high solar concentration and elevated temperatures for hybrid solar thermal-photovoltaic power plants," *Prog. Photovoltaics, Res. Appl.*, vol. 28, no. 11, pp. 1167–1174, Nov. 2020, doi: 10.1002/pip.3326.

[12] Y. Zhao et al., "InGaN-based solar cells for space applications," in *Proc. Midwest Symp. Circuits Syst.*, Aug. 2017, pp. 954–957.

[13] X. Huang et al., "Reliability analysis of InGaN/GaN multi-quantum-well solar cells under thermal stress," *Appl. Phys. Lett.*, vol. 111, no. 23, Dec. 2017, Art. no. 233511, doi: 10.1063/1.5006650.

[14] A. Caria et al., "GaN-based high-periodicity multiple quantum well solar cells: Degradation under optical and electrical stress," *Microelectron. Rel.*, vol. 114, Nov. 2020, Art. no. 113802, doi: 10.1016/j.microrel.2020.113802.

[15] M. Nicoletto et al., "Role of p-GaN layer thickness in the degradation of InGaN-GaN MQW solar cells under 405 nm laser excitation," *Microelectron. Rel.*, vol. 138, Nov. 2022, Art. no. 114727, doi: 10.1016/j.microrel.2022.114727.

[16] P. Dalapati, K. Yamamoto, T. Egawa, and M. Miyoshi, "Understanding the degradation mechanisms of InGaN/GaN multiple quantum well UV photodetectors submitted to different current stresses," *Opt. Lett.*, vol. 46, no. 15, p. 3568, Aug. 2021, doi: 10.1364/OL.434920.

[17] P. Dalapati et al., "Current-induced degradation behaviors of InGaN/GaN multiple quantum well UV photodetectors: Role of electrically active defects," *Sens. Actuators A, Phys.*, vol. 347, Nov. 2022, Art. no. 113935, doi: 10.1016/j.sna.2022.113935.

[18] X. Huang et al., "Energy band engineering of InGaN/GaN multi-quantum-well solar cells via AlGaN electron- and hole-blocking layers," *Appl. Phys. Lett.*, vol. 113, no. 4, Jul. 2018, Art. no. 043501, doi: 10.1063/1.5028530.

[19] A. Armstrong, T. A. Henry, D. D. Koleske, M. H. Crawford, K. R. Westlake, and S. R. Lee, "Dependence of radiative efficiency and deep level defect incorporation on threading dislocation density for InGaN/GaN light emitting diodes," *Appl. Phys. Lett.*, vol. 101, no. 16, Oct. 2012, Art. no. 162102, doi: 10.1063/1.4759003.

[20] M. Mandurrino et al., "Physics-based modeling and experimental implications of trap-assisted tunneling in InGaN/GaN light-emitting diodes," *Phys. Status Solidi*, vol. 212, no. 5, pp. 947–953, May 2015, doi: 10.1002/pssa.201431743.

[21] M. A. der Maur, B. Galler, I. Pietzonka, M. Strassburg, H. Lugauer, and A. D. Carlo, "Trap-assisted tunneling in InGaN/GaN single-quantum-well light-emitting diodes," *Appl. Phys. Lett.*, vol. 105, no. 13, 2014, Art. no. 133504, doi: 10.1063/1.4896970.

[22] L. Liu, M. Ling, J. Yang, W. Xiong, W. Jia, and G. Wang, "Efficiency degradation behaviors of current/thermal co-stressed GaN-based blue light emitting diodes with vertical-structure," *J. Appl. Phys.*, vol. 111, no. 9, May 2012, Art. no. 093110, doi: 10.1063/1.4712030.

[23] M. Meneghini, L. R. Trevisanello, U. Zehnder, G. Meneghesso, and E. Zanoni, "Reversible degradation of ohmic contacts on p-GaN for application in high-brightness LEDs," *IEEE Trans. Electron Devices*, vol. 54, no. 12, pp. 3245–3251, Dec. 2007, doi: 10.1109/TED.2007.908900.

[24] M. Meneghini, L. Trevisanello, U. Zehnder, G. Meneghesso, and E. Zanoni, "Thermal degradation of InGaN/GaN LEDs ohmic contacts," *Phys. Status Solidi C*, vol. 5, no. 6, pp. 2250–2253, May 2008, doi: 10.1002/PSSC.200778654.

[25] A. Caria et al., "Excitation intensity and temperature-dependent performance of InGaN/GaN multiple quantum wells photodetectors," *Electronics*, vol. 9, no. 11, p. 1840, Nov. 2020, doi: 10.3390/electronics9111840.

[26] M. Auf der Maur, G. Moses, J. M. Gordon, X. Huang, Y. Zhao, and E. A. Katz, "Temperature and intensity dependence of the open-circuit voltage of InGaN/GaN multi-quantum well solar cells," *Sol. Energy Mater. Sol. Cells*, vol. 230, Sep. 2021, Art. no. 111253, doi: 10.1016/j.solmat.2021.111253.

[27] W. Shockley and W. T. Read Jr., "Statistics of the recombinations of holes and electrons," *Phys. Rev.*, vol. 87, pp. 835–842, Sep. 1952, doi: 10.1103/PhysRev.87.835.

[28] M. Meneghini et al., "Characterization of the deep levels responsible for non-radiative recombination in InGaN/GaN light-emitting diodes," *Appl. Phys. Lett.*, vol. 104, no. 11, Mar. 2014, Art. no. 113505, doi: 10.1063/1.4868719.

[29] C. G. Van de Walle, "Interactions of hydrogen with native defects in GaN," *Phys. Rev. B, Condens. Matter*, vol. 56, no. 16, pp. R10020–R10023, Oct. 1997, doi: 10.1103/PhysRevB.56.R10020.

[30] C. E. Dreyer, A. Alkauskas, J. L. Lyons, J. S. Speck, and C. G. Van de Walle, "Gallium vacancy complexes as a cause of shockley-read-Hall recombination in III-nitride light emitters," *Appl. Phys. Lett.*, vol. 108, no. 14, Apr. 2016, Art. no. 141101, doi: 10.1063/1.4942674.

[31] S. F. Chichibu et al., "The origins and properties of intrinsic nonradiative recombination centers in wide bandgap GaN and AlGaN," *J. Appl. Phys.*, vol. 123, no. 16, Apr. 2018, Art. no. 161413, doi: 10.1063/1.5012994.

[32] M. Meneghini et al., "GaN-based power devices: Physics, reliability, and perspectives," *J. Appl. Phys.*, vol. 130, no. 18, Nov. 2021, Art. no. 181101, doi: 10.1063/5.0061354.

[33] M. Buffolo et al., "Defects and reliability of GaN-based LEDs: Review and perspectives," *Phys. Status Solidi A*, vol. 219, no. 8, Apr. 2022, Art. no. 2100727, doi: 10.1002/PSSA.202100727.

[34] R. A. Sinton and A. Cuevas, "Contactless determination of current–voltage characteristics and minority-carrier lifetimes in semiconductors from quasi-steady-state photoconductance data," *Appl. Phys. Lett.*, vol. 69, no. 17, pp. 2510–2512, Oct. 1996, doi: 10.1063/1.117723.

Authorized licensed use limited to: Fondren Library Rice University. Downloaded on August 24,2023 at 15:03:13 UTC from IEEE Xplore. Restrictions apply.